DOI: 10.1002/cctc.201200045

Theoretical Study of Asymmetric Transfer Hydrogenation of Ketones Catalyzed by Amino Acid-Derived Rhodium Complexes

Mikael Nordin,[a] Rong-Zhen Liao,[b] Katrin Ahlford,[a] Hans Adolfsson,*[a] and Fahmi Himo*[a]

Density functional theory calculations are employed to study the asymmetric transfer hydrogenation of ketones catalyzed by rhodium–arene complexes containing hydroxamic acid-functionalized amino acid ligands. Firstly, the ligand–metal binding is investigated and it is shown that both the N,N and O,O binding modes Are viable. For each of these, the full free energy profile for the transfer hydrogenation is calculated according to the outer-sphere reaction mechanism. Three factors are demonstrated to influence the stereoselectivity of the process, namely the energy difference between the metal–ligand binding modes, the energy difference between the intermediate hydrogenated catalyst, and the existence of a stabilizing CH–π interaction between the Cp* ligand of the catalyst and the phenyl moiety of the substrate. Theoretical reproduction of the selectivity of a slightly modified ligand that is shown experimentally to yield the opposite enantioselectivity corroborates these results. Finally, a technical observation made is that inclusion of dispersion interactions (using the B3LYP-D2 correction or the M06 functional) proved to be very important for reproducing the enantioselectivity.

Introduction

Asymmetric reduction of prochiral ketones is a highly efficient route towards the formation of enantiomerically enriched secondary alcohols.[1] Transition metal-catalyzed asymmetric transfer hydrogenation (ATH) with 2-propanol or formic acid as reducing agents is a powerful alternative to methods based on catalytic hydrogenation, or the use of main group hydride reagents.[2] In a transfer hydrogenation reaction, the substrate formally accepts a proton and a hydride from the reducing agent. In ketone reductions performed with 2-propanol as reducing agent, there is a simultaneous formation of acetone along with the production of the desired secondary alcohol. A number of different catalyst systems have been developed for the ATH reaction. The most commonly employed catalysts are based on complexes, which are often generated in situ, of either ruthenium(II)–, rhodium(III)–, or iridium(III)–arene precursors with either monoprotected vicinal diamines or amino alcohols as ligands.[3] The generally accepted mechanism for ATH using these catalysts is the "outer-sphere mechanism", in which the bifunctional transition metal catalyst acts as both hydride and proton donor (Figure 1).[2d,4] The key to success with these kinds of catalysts is the inherent properties of the catalytically active metal complexes. For an efficient transfer hydrogenation, in which the catalyst accepts a hydride from the reducing agent, the catalyst requires an acidic site. In these complexes the transition metal acts as the Lewis acidic site, accepting the hydride. At the same time, the removal of a proton from the reducing agent requires a basic site, and the coordinated amine performs the deprotonation. In addition, the successfully employed diamine or amino alcohol ligands contain an acidic site (e.g., NHTs and OH, respectively), which ionize easily and form strong interactions with the transition metal under the reaction conditions.

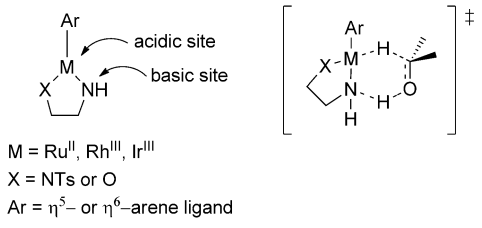

Figure 1. General structure of the best catalysts for the asymmetric transfer hydrogenation of ketones, and the six-membered outer-sphere transition state postulated for the hydride- and proton-transfer from and to the catalyst.

We have demonstrated that ruthenium and rhodium catalysts based on α-amino acid-derived ligands are highly efficient and selective in the ATH of aryl alkyl ketones in 2-propanol.[5] The use of a catalyst combination of the hydroxamic acid-functionalized L-valine (**1**) together with $[RhCp^*Cl_2]_2$ gave the secondary alcohols in high enantioselectivity with the *S*-configuration (Scheme 1).[6] Employing the corresponding thioamide (**2**) as a ligand resulted again in high product enantioselectivity, albeit with *R*-configuration.[7] Clearly, a small change in the ligand structure related to possible donor atoms resulted in

[a] *M. Nordin, Dr. K. Ahlford, Prof. H. Adolfsson, Prof. F. Himo*
Department of Organic Chemistry
Arrhenius Laboratory, Stockholm University
SE-10691 Stockholm, Sweden
E-mail: hansa@organ.su.se
himo@organ.su.se

[b] *Dr. R.-Z. Liao*
Max-Planck-Institut für Kohlenforschung
Kaiser-Wilhelm-Platz 1, D-45470
Mühlheim an der Ruhr (Germany)

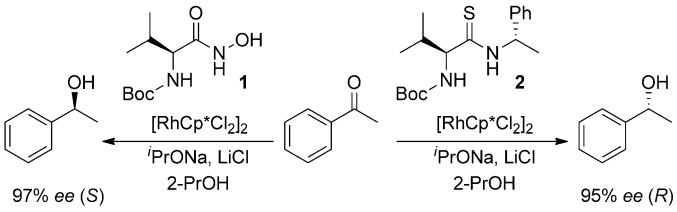

Scheme 1. Rh-catalyzed ATH of aryl alkyl ketones with $[RhCp^*Cl_2]_2$ and hydroxamic acid-functionalized L-valine (**1**) or thioamide (**2**) catalyst combinations.

the opposite product selectivity. To clarify the underlying reasons for the behavior of the individual catalytic systems, a number of mechanistic studies were performed.[6b] A difference between the amino acid-based ligands and catalysts containing diamine or amino alcohol ligands is the apparent lack of a basic site. The acidic, and thereby easily ionizable, sites in ligands **1** and **2** are the hydroxamic acid and the thioamide functional groups, respectively, based on their pK_a-values. These functional groups should, therefore, be equivalent to the sulfonamide or the alcohol in the ligands depicted in Figure 1. In comparison to an amine, the corresponding carbamate-protected amine (Boc–NH) should possess very poor basic properties in its neutral form, and would act as a proton acceptor after an initial ionization. The ATH reaction catalyzed by the rhodium–arene complexes with ligand **1** or **2** requires an excess of base, typically 5–10 equivalents of sodium isopropoxide relative to the amount of catalyst, for a successful reaction outcome. Therefore, the amount of base present in the reaction mixture should be enough for securing deprotonation of both functionalities of the ligands upon interaction with the catalytically active rhodium ion.

To further investigate the contrasting outcomes in the absolute configuration of the product alcohol for the two catalytic systems (i.e., with ligands **1** or **2**), we performed a series of kinetic investigations. These studies revealed that the rate constants for the two systems differed substantially. Based on the obtained rate constants, we calculated the initial rates for the individual reaction steps (i.e., Rh–H formation and substrate reduction) and found the rate-determining steps for the two systems to be different. For the hydroxamic acid-containing system, the formation of the rhodium hydride intermediate was found to be rate-determining, whereas, for the corresponding thioamide system, the transfer of a hydride from the catalyst to the substrate was the slow reaction step.

The different kinetic behavior of the two catalyst systems could be the reason for the generation of products of opposite configuration. However, the data obtained from experimental studies are, unfortunately, not sufficient enough for a conclusive picture of the reaction.

In this paper, we focus on the catalytic systems with ligand **1** and use DFT calculations to investigate the mechanism and source of enantioselectivity in the ATH reaction. A detailed understanding of the reaction mechanism could contribute to catalyst optimization for transfer hydrogenation of ketones and imines with respect to increased product stereoselectivity and reduced catalyst loading.

Results and Discussion

As discussed in the Introduction, previous mechanistic studies on related systems have shown that the bifunctional outer-sphere monohydride mechanism for transfer hydrogenation is favored over other mechanisms.[4] In this mechanism, the transition states adopt six-membered cyclic structures, in which the transfer of hydride and proton occurs concomitantly. We will, therefore, restrict the study to this pathway in the present work and focus on the properties of the particular combination of metal (Rh) and ligand (hydroxamic acid **1**) system. Firstly, we discuss the relative energies of the various binding modes that the ligand can adopt. The transfer hydrogenation reaction will then be studied for the two most stable modes And all possible transition states leading to the different products will be discussed. Finally, the transfer hydrogenation transition states for a modified ligand, which has been shown experimentally to yield the opposite enantiomer of the product compared to hydroxamic acid **1**, will be discussed to further corroborate the conclusions.

Notably, a thorough conformational analysis was undertaken at each stage, owing to the flexible *i*Pr, Boc, and Bn sidechains of ligands **1** and **3**. Only the lowest energy structures are presented.

Ligand binding modes

A number of different reasonable binding modes for the hydroxamic acid ligand **1** to the metal center are possible, as shown in Figure 2. These complexes share the η^2-binding to Rh^{III} to form 16-electron complexes. Their relative energies are indicated in the scheme, and the optimized structures and detailed energy breakdowns are given in the Supporting Information.

Binding modes A and B are clearly more stable than the other ones. The N,N binding mode A has been suggested previously, based on experimental findings,[6b] whereas the O,O binding mode B was not considered a viable option, owing

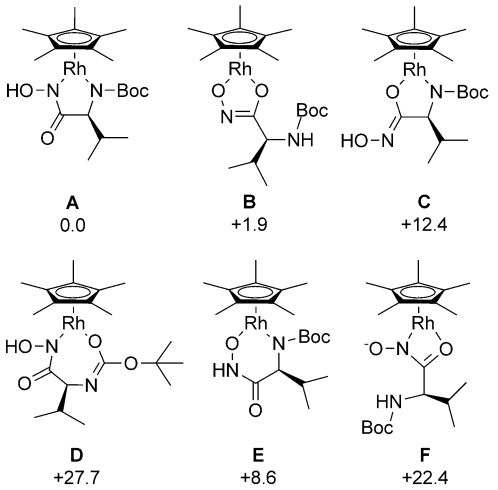

Figure 2. Different ligand binding modes And their calculated relative free energies in kcal mol^{-1}.

mainly to the greater distance between the ligand stereocentre and the bifunctional site, which would hinder the induction of the high stereoselectivity that was observed experimentally. Considering energetic factors, however, mode B is comparable to A as it is only 1.9 kcal mol^{-1} higher and cannot be ruled out at this stage. The reactions of both binding modes must, therefore, be considered.

Reaction with binding mode A

Hydrogenation of the catalyst by 2-propanol is possible from two sides of the catalyst metal–ligand chelate ring, resulting in the formation of two metal hydride diastereomers, with Rh(*R*) or Rh(*S*) configurations. The optimized transition state structures for hydrogenation of the catalyst (A-TS 1-R and A-TS 1-S) as well as the corresponding hydrogenated catalysts (A-Int-R and A-Int-S) are shown in Figure 3.

In line with previous theoretical studies of transfer hydrogenation reactions,[4] we find that the reaction takes place through a concerted six-membered cyclic transition state in which the hydride is transferred to the metal center and the proton to the nitrogen of the ligand. A-TS 1-R is calculated to be 24.9 kcal mol^{-1} higher than the separate reactants (catalyst + 2-propanol), whereas A-TS 1-S lies at +28.9 kcal mol^{-1}.

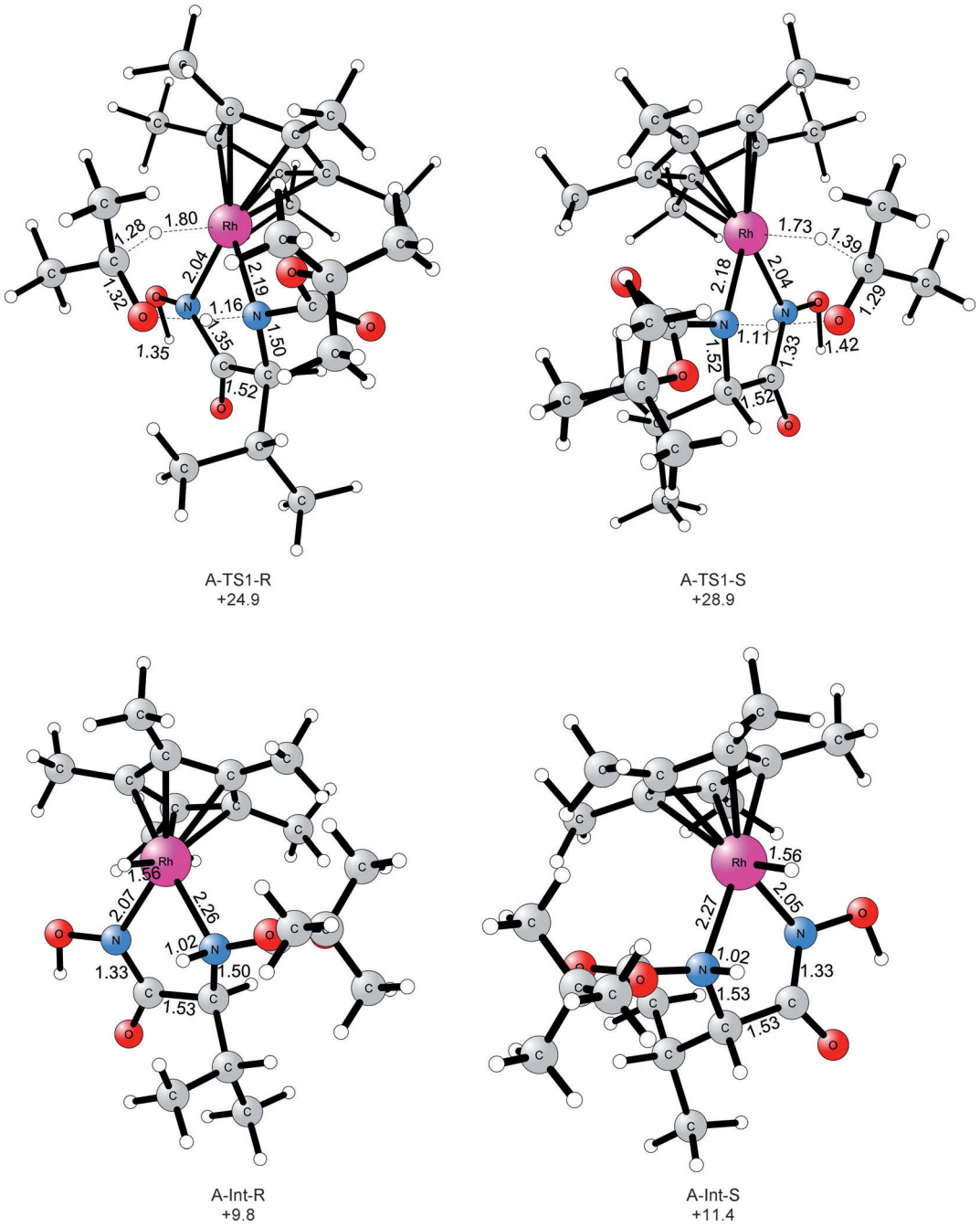

Figure 3. Optimized structures of transition states for hydrogenation of the metal–ligand ring from both sides (A-TS 1-R and A-TS 1-S) and the resulting hydrogenated catalyst intermediates (A-Int-R and A-Int-S). Distances are in Å; free energies are in kcal mol^{-1} and relative to the separate reactants.

The reason for this preference is that in transition state A-TS 1-S, the isopropyl group of the ligand clashes with Cp* (see Figure 3). This repulsion is also reflected, but to a lesser extent, in the energy differences for the hydrogenated catalyst, that is, for A-Int-R and A-Int-S, which are calculated to be +9.8 and +11.4 kcal mol^{-1} higher than the reactants, respectively.

Experimentally, the first step has a measured rate constant of 0.198 min^{-1}, which corresponds to a reaction barrier of approximately 21 kcal mol^{-1}. The rate constant for the reverse reaction is measured at 69.4 min^{-1}, which indicates that the reaction step is endothermic by 3.5 kcal mol^{-1}.[6b] The calculated barrier and endothermicity of the first step are, thus, both overestimated compared to the experimental values.

The second reaction step is the asymmetric reduction of acetophenone by the hydrogenated catalyst. Each of the two metal hydrides can reduce the prochiral substrate from its *re* or *si* face, resulting in a total of four transition states, here termed A-TS2-RS, A-TS2-SS, A-TS2-RR, and A-TS2-SR. The former two correspond to *re* face reduction to form (*S*)-1-phenylethanol, whereas the latter two correspond to *si* face reduction to afford (*R*)-1-phenylethanol. We have optimized these four TSs and they are displayed in Figure 4. The calculated bar-

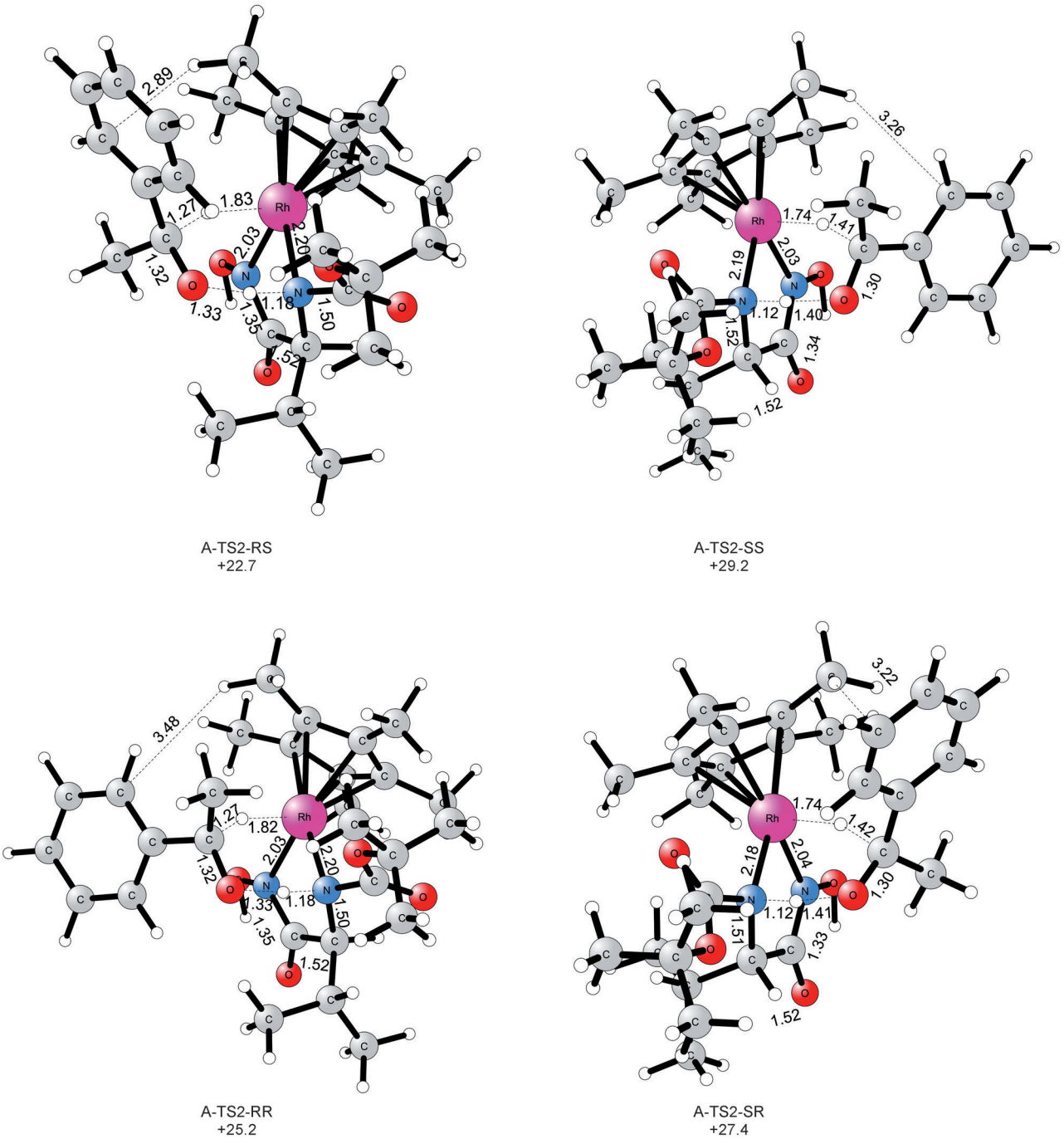

Figure 4. Optimized transition state structures for the asymmetric reduction of acetophenone by hydrogenated catalyst in binding mode A. Distances are in Å; free energies are in kcal mol^{-1} and relative to the separate reactants (A + 2-propanol).

riers relative to the reactants (unhydrogenated catalyst + 2-propanol) are also indicated in the figure and a summary of the resulting energy graph for the entire reaction is shown in Figure 5.

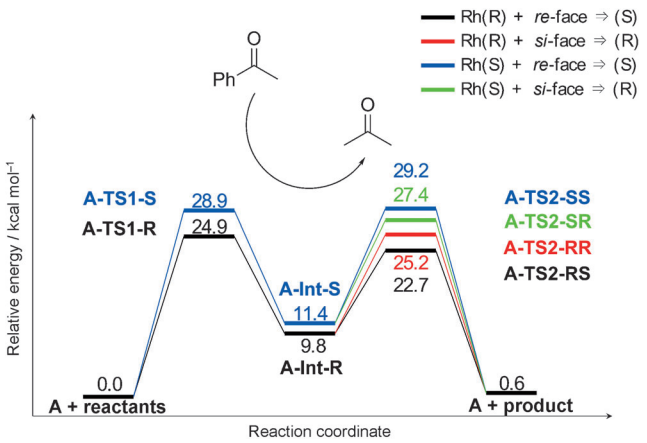

Figure 5. Overall free energy curves for the asymmetric transfer hydrogenation reaction of acetophenone with the catalyst in binding mode A. Free energies are in kcal mol^{-1} and relative to the separate reactants (A + 2-propanol).

The lowest *S* and *R* products are both formed from the Rh(*R*)-hydrogenated catalyst, that is, from A-Int-R, because the Rh(*S*)-hydrogenated catalyst suffers from the above-mentioned steric repulsion between the isopropyl group and Cp*. Consistent with the experimental findings, the lowest barrier is observed for the formation of the *S* product (A-TS2-RS, + 22.7 kcal mol^{-1}), which is 2.5 kcal mol^{-1} lower than the lowest transition state leading to the *R* product (A-TS2-RR, + 25.2 kcal mol^{-1}). By comparing the structures of these two transition states, we can trace the energy difference to a stabilizing CH–π interaction between a methyl group of Cp* and the phenyl ring of the substrate; this is not present in the TS in which the hydrogenation takes place at the *si* face of the substrate. This is analogous to the explanations provided by Noyori et al. for the ruthenium catalysts[4a,b] and by Andersson et al.[4d]

In this binding mode, the stereoselectivity is, therefore, a result of a combination of the repulsive isopropyl–Cp* interaction present in the hydrogenated catalyst, and the attractive Cp*–phenyl interaction present in the transition state.

Finally, the overall reaction, Equation (1):

$$\text{2-propanol} + \text{acetophenone} \rightarrow \text{acetone} + \text{1-phenylethanol} \quad (1)$$

is calculated to be endothermic by 0.6 kcal mol^{-1}, which agrees with the experimental finding that the reaction is reversible.

Reaction with binding mode B

As discussed above, the O,O binding mode B is calculated to be 1.9 kcal mol^{-1} higher than mode A. This energy difference will, therefore, be added to all of the barriers and intermediate energies obtained for this binding mode.

Analogously to binding mode A, hydrogenation of the catalyst in binding mode B can take place from both sides of the rhodium–ligand chelate ring, resulting in the formation of metal hydrides with Rh(*R*) or Rh(*S*) configurations. The optimized transition state structures and the resulting hydrogenated catalysts are very similar to those of binding mode A and are given in the Supporting Information.

In this O,O binding mode, the oxygen center of the ligand functions as the proton acceptor. Formation of Rh(*R*) proceeds via B-TS 1-R with a calculated overall barrier of 24.3 kcal mol^{-1} relative to the separate reactants of the lowest binding mode (i.e., catalyst in binding mode A and 2-propanol), whereas formation of Rh(*S*) via B-TS 1-S has a barrier of 25.7 kcal mol^{-1}. The energy difference is calculated to be 1.4 kcal mol^{-1}, which is considerably lower than the 4.0 kcal mol^{-1} obtained for the corresponding transition states in binding mode A. The reason for the observed difference can be explained by the fact that the chiral center in mode B is located further away from the metal and the Cp* ligand. The energies of the resulting hydrogenated catalysts B-Int-R and B-Int-S are 10.5 and 11.6 kcal mol^{-1} higher than the reactants, respectively.

The optimized structures of the four transition states for the asymmetric reduction of acetophenone are displayed in Figure 6 and the overall energy profile calculated for binding mode B, in Figure 7. In binding mode B the lowest barrier is also obtained for the formation of the *S* product (B-TS 2-RS, + 23.7 kcal mol^{-1}), which now is only 0.9 kcal mol^{-1} lower than the lowest transition state leading to the *R* product (B-TS 2-SR, + 24.6 kcal mol^{-1}).

However, since the absolute barriers of the two binding modes Are very close, one should compare them to study the sources of the enantioselectivity. By comparing Figures 5 and 7, one can see that the lowest-lying TS leading to the *S* product stems from binding mode A (A-TS 2-RS with a barrier of 22.7 kcal mol^{-1}), whereas the lowest-lying TS leading to the *R* product stems from mode B (B-TS 2-SR with a barrier of 24.6 kcal mol^{-1}). The energy difference is 1.9 kcal mol^{-1}, which is consistent with the experimentally determined enantioselectivity of 87% (97% *ee* with LiCl addition).

Hence, these results show that both binding modes contribute to the overall selectivity of the ligand and must be considered explicitly to reproduce the experimental results. Any alterations in the ligand might affect the selectivity by changing the relative binding energies of the two modes, in addition, of course, to the other effects discussed above, that is, the repulsive isopropyl–Cp* interaction present in the hydrogenated catalyst and the attractive Cp*–phenyl interaction present in the transition state.

Stereoselectivity with ligand 3

To test the ideas presented above regarding stereoselectivity, we studied a modified ligand (hydroxamic acid **3**, Scheme 2) that was shown experimentally to lead to the opposite product stereoselectivity (34% *ee* (*R*) and 64% conversion with LiCl; 21% *ee* (*R*) and 13% conversion without LiCl) in comparison to the ligand studied hitherto (ligand **1**).[6b] Hydroxamic acid

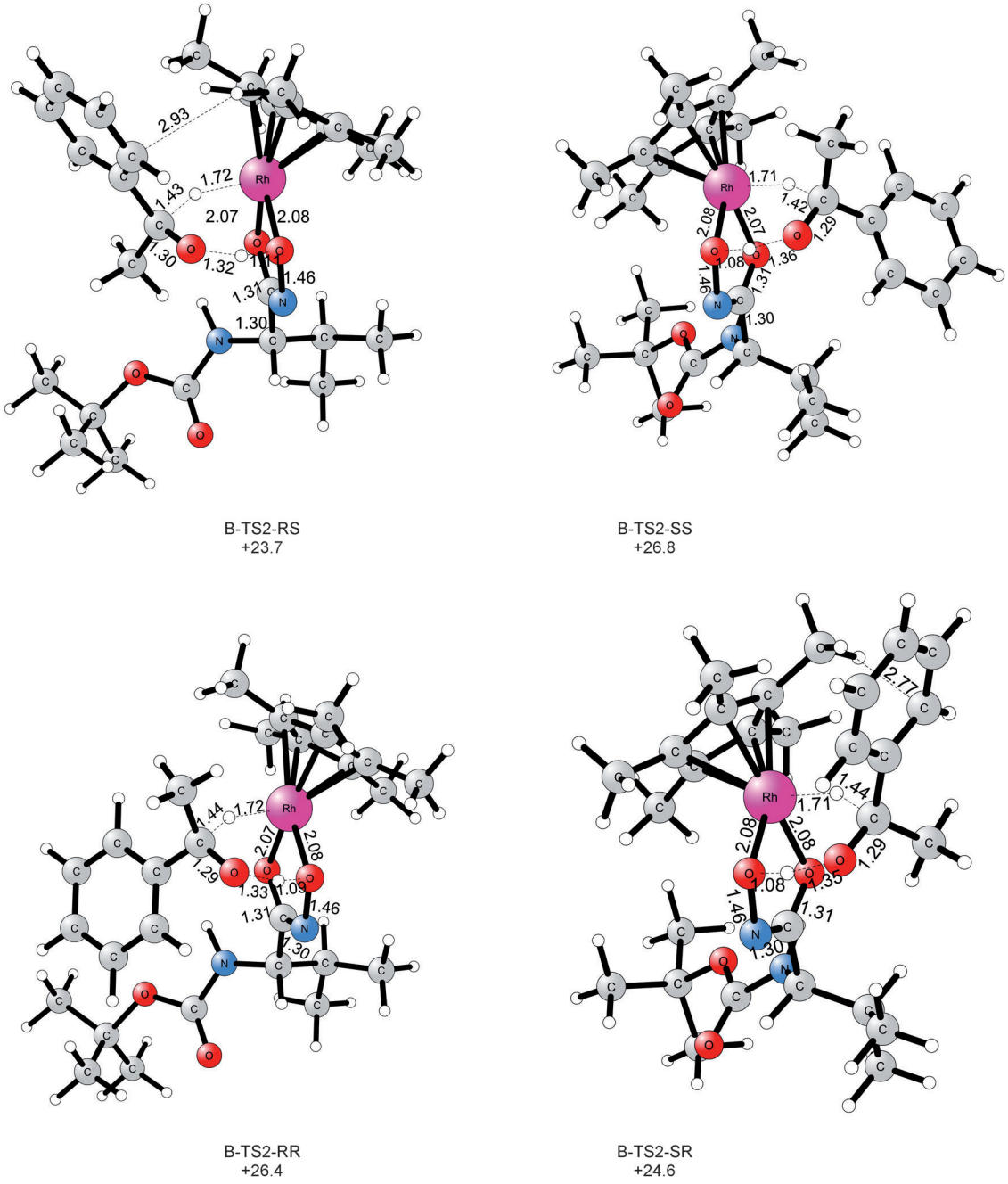

Figure 6. Optimized transition state structures for the asymmetric reduction of acetophenone by hydrogenated catalyst in binding mode B. Distances are reported in Å; free energies are in kcal mol^{-1} and relative to the separate reactants in binding mode A (A + 2-propanol).

ligand **3** differs from the previously studied ligand **1** on two accounts. It is derived from the amino acid L-phenylalanine instead of L-valine; moreover, it lacks the Boc protection group present in ligand **1**.

Similar to the previous case, the N,N and O,O binding modes (called 3A and 3B) are calculated to be lowest in energy for this ligand, with the former being 3.4 kcal mol^{-1} lower in energy (see Supplementary Information for details on the energies of the various binding modes And the optimized structures). For each of the two binding modes we have calculated the four stereo-determining transition states for reduction of acetophenone (corresponding to the Rh(*R*) or Rh(*S*) configurations of the catalyst and hydrogenation of the *re* or *si* faces of the substrate). The calculated barriers (as before, relative to the most stable complex of catalyst and 2-propanol) are given in Table 1.

The calculations show that the N,N binding mode 3A has considerably lower barriers for hydrogenating the substrate compared to the O,O binding mode 3B (more than 12 kcal mol^{-1}). In the N,N binding mode, removal of the Boc group leads to a more electron-rich metal center that is more prone to donate the hydride, whereas in the O,O binding mode, re-

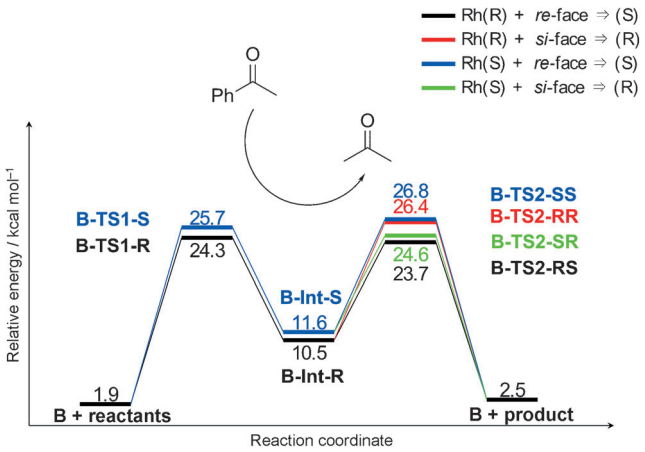

Figure 7. Overall free energy curves for the asymmetric transfer hydrogenation reaction catalyzed by catalyst in binding mode B. Free energies are in kcal mol^{-1} and relative to the reactants of binding mode A.

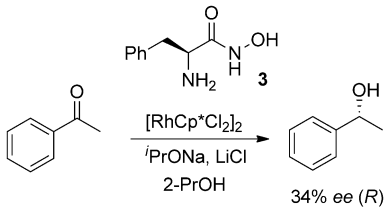

Scheme 2. Rh-catalyzed ATH with modified hydroxamic acid ligand **3**.

Table 1. Calculated free energy barriers for the stereo-determining TS 2 for ligand **3** in the binding modes 3 A and 3 B.

TS	Absolute barrier [kcal mol^{-1}]	Relative barrier [kcal mol^{-1}]
3 A-TS 2-RS	14.0	+1.1
3 A-TS 2-SS	16.4	+3.5
3 A-TS 2-RR	15.6	+2.7
3 A-TS 2-SR	12.9	0.0
3 B-TS 2-RS	25.7	+12.8
3 B-TS 2-SS	27.9	+15.0
3 B-TS 2-RR	25.9	+13.0
3 B-TS 2-SR	26.8	+13.9

moval of the Boc group has no effect on the properties of the metal. The optimized structures of the transition states of binding mode 3 A are shown in Figure 8 and the TS structures of mode 3 B are given in the Supporting Information.

Most importantly, the calculations correctly reproduce the fact that this ligand affords the *R* form of the product. 3 A-TS 2-SR is 1.1 kcal mol^{-1} lower than 3 A-TS 2-RS, which corresponds quite well with the experimental findings. Both of these transition states have the advantageous stabilizing CH–π electrostatic interaction between the Cp* of the catalyst and the phenyl ring of the substrate. However, in the case of 3 A-TS 2-SR there is an additional similar attractive CH–π interaction between the Cp* and the phenyl substituent of the ligand (see Figure 8), which causes the energy of this TS to be lower and, thus, determines the selectivity.

These results, in particular the fact that the calculations reproduce and rationalize the stereoselectivity of ligand **3**, provide further corroboration to the results presented above for ligand **1**.

Effect of dispersion on selectivity

An important technical issue is the influence of dispersion on the relative TS energies and, thus, the selectivity. Most DFT functionals suffer from the lack of description of the attractive dispersion interaction. It has recently been shown that addition of dispersion corrections to the B3LYP functional improves the results considerably in a number of diverse applications.[8]

In the case of the Rh-catalyzed asymmetric transfer hydrogenation reaction studied here, we found that inclusion of dispersion was important for reproduction of the enantioselectivity. In Table 2 are listed the relative energies of the stereo-determining TS 2 for ligands **1** and **3** with (B3LYP-D2)[9] and without (B3LYP)[10] the dispersion correction, along with single-point energies calculated using the M06 functional,[11] which includes noncovalent interactions in its training set.

The first striking observation is that for the bulkier *N*-Boc protected hydroxamic acid ligand **1**, the dispersion correction stabilized the transition states of mode A considerably more than those of mode B, in the order of 12–13 kcal mol^{-1}. The M06 functional gives a very similar picture, which corroborates these results. Concerning the enantioselectivity of this ligand, the energy difference between the lowest-lying transition states leading to the two different products is increased from 0.8 kcal mol^{-1} between B-TS 2-RS and B-TS 2-SR to 1.9 kcal mol^{-1} between A-TS 2-RS and B-TS 2-SR (M06 gives 1.4 kcal mol^{-1}). The latter values are in better agreement with the experimentally observed selectivity.

For ligand **3**, dispersion has much smaller effects on the energy difference between the transition states belonging to the two different binding modes. Without dispersion, the 3 A-TS 2-RS leading to the wrong *S* enantiomer of the product is the lowest in energy, whereas, with dispersion, the order is reversed and 3 A-TS 2-SR, which gives the correct *R* enantiomer of the product, is the lowest in energy. Without inclusion of the dispersion correction, B3LYP fails to reproduce the experimentally observed selectivity, whereas both B3LYP-D2 and M06 give the correct ordering of the transition states.

These results further demonstrate the importance of the dispersion correction to the well-established B3LYP functional.

Conclusion

In the present study, the rhodium-catalyzed asymmetric reduction of acetophenone was investigated by means of DFT calculations. Two amino acid-based ligands were considered. For the first one, ligand **1** (Scheme 1), the full catalytic cycle was studied according to the well-established outer-sphere reaction mechanism. For the other modified ligand **3** (Scheme 2), which was shown experimentally to yield the opposite enan-

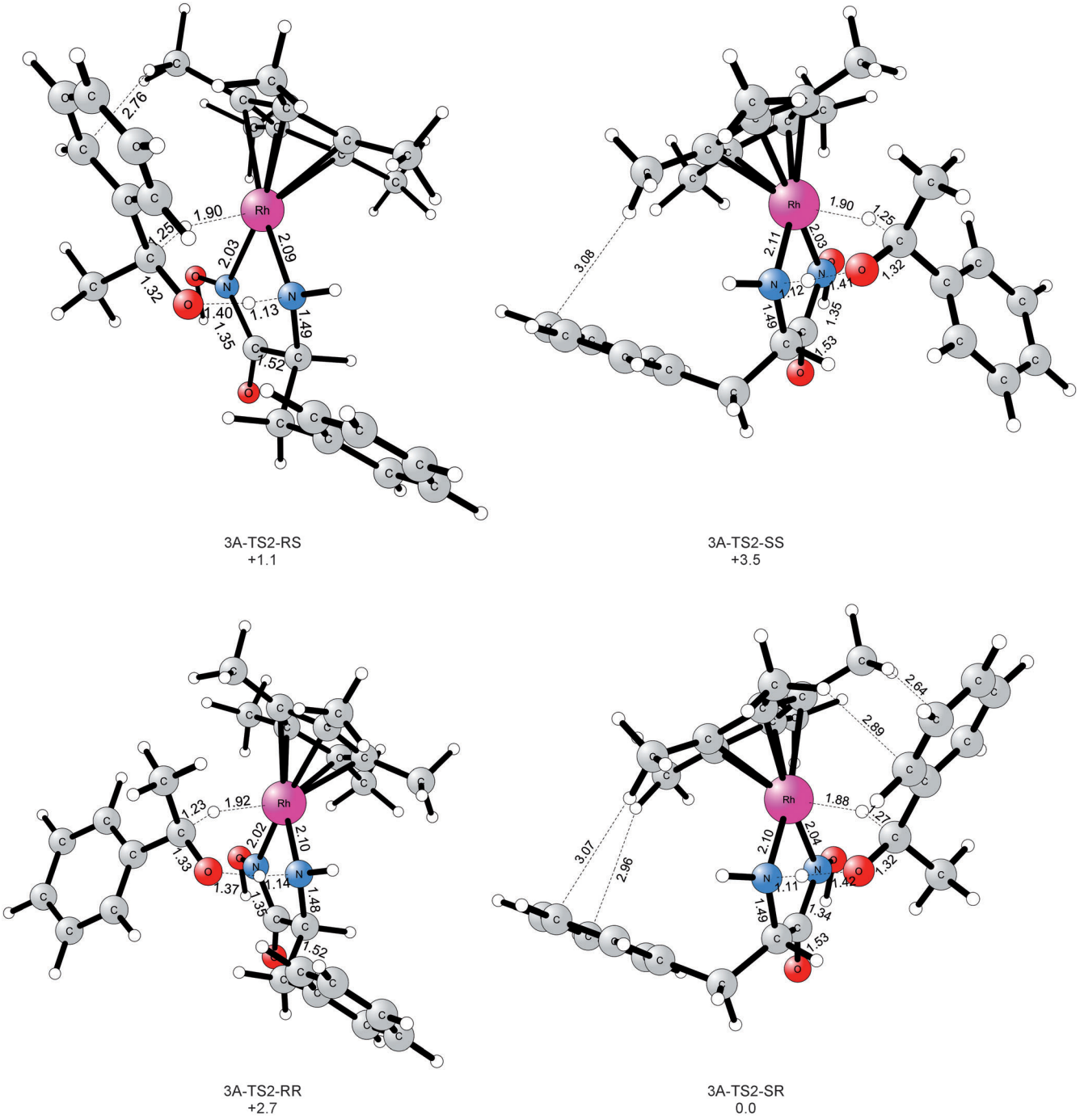

Figure 8. Optimized transition state structures for the reduction of acetophenone by hydrogenated catalyst with ligand 3 in binding mode 3 A (N,N). Their relative free energies are given in kcal mol^{-1}.

tioselectivity, only the stereoselectivity-determining transition states were analyzed.

The DFT calculations reproduce the experimental selectivities for both ligands and also provide rationalization to the observations. For each ligand, a number of plausible binding modes to the metal were considered and it was shown that both N,N and O,O bindings are energetically accessible and must be considered for the overall catalytic process.

The first step of the reaction, the hydrogenation of the metal center by 2-propanol, is possible from two sides of the catalyst metal–ligand chelate ring, resulting in the formation of two metal hydride diastereomers, with Rh(*R*) or Rh(*S*) configurations. The energy difference between the two depends on the ligand and the particular choice of substituents and contributes to the selectivity of the second step, that is, the stereo-determining hydrogenation of acetophenone.

Table 2. Effect of including dispersion effects on relative transition state free energies.[a]

TS	B3LYP [kcal mol^{-1}]	B3LYP-D2 [kcal mol^{-1}]	M06 [kcal mol^{-1}]
		Ligand ***1***	
A-TS 2-RS	0.0	0.0	0.0
A-TS 2-SS	+5.5	+6.5	+7.8
A-TS 2-RR	+1.2	+2.5	+2.0
A-TS 2-SR	+4.7	+4.7	+6.1
B-TS 2-RS	−12.0	+1.0	0.0
B-TS 2-SS	−9.2	+4.1	+3.7
B-TS 2-RR	−7.8	+3.8	+3.5
B-TS 2-SR	−11.2	+1.9	+1.4
		Ligand ***3***	
3A-TS 2-RS	0.0	0.0	0.0
3A-TS 2-SS	+5.0	+2.4	+1.5
3A-TS 2-RR	+0.5	+1.6	+0.4
3A-TS 2-SR	+1.9	−1.1	−1.3
3B-TS 2-RS	+10.0	+11.7	+11.7
3B-TS 2-SS	+8.9	+13.9	+13.4
3B-TS 2-RR	+10.0	+11.9	+11.8
3B-TS 2-SR	+9.5	+12.8	+12.5

[a] Single point calculations on B3LYP-optimized geometries, employing basis sets consisting of SDD for Rh and 6-311+G(2d,2p) for all other elements. Zero-point and solvation energies are included for all methods at the B3LYP/sdd,6-31G(d,p) level.

In the second step, a stabilizing CH–π interaction between a methyl group of the Cp* ligand and the phenyl ring of the substrate exists on hydrogenation from either the *re* or the *si* face of the substrate with both ligands **1** and **3**, which contributes to stereoselectivity.

The balance between these three factors, that is, the energy of the ligand binding mode, the energy difference between the metal hydride diastereomers, and the CH–π interaction, will ultimately determine the stereochemical outcome of the reaction. These results suggest, therefore, that it is not straightforward to predict how alterations of the ligand or substrate will affect the enantioselectivity, because even subtle changes may influence all three factors in different ways, which can have severe consequences for the enantioselectivity.

Finally, a technical point is that inclusion of dispersion correction to the B3LYP functional is very important for reproduction of the selectivity.

Computational Methods

All calculations reported were performed using DFT employing the B3LYP hybrid functional, as implemented in the Gaussian 03 software package.[12] Geometries were optimized using the 6-31G(d,p) basis set for all elements, except rhodium, for which the SDD effective core potential was employed.[13] Based on the optimized geometries, single-point calculations using SDD for Rh and the larger 6-311+G(2d,2p) for the other elements were performed to obtain more accurate energies. Frequency calculations were performed at the same theory level as the geometry optimizations.

The reported energies are Gibbs free energies, which include zero-point vibrational corrections, thermal corrections at 298 K and solvation free energies. The solvation energies were calculated as single-point corrections on the optimized structures using the conductor-like polarizable continuum model method,[14] with dielectric constant $\varepsilon = 19.264$ for 2-propanol and the cavities formed according to UAKS (using ethanol). In addition, dispersion corrections were included using the B3LYP-D2 method, as recent studies showed inclusion of these effects to significantly improve the performance of the B3LYP functional. For comparison, selected transition state energies were also calculated using the M06 functional (as implemented in Gaussian 09),[15] which includes noncovalent interactions in its training set.

Acknowledgements

F.H. acknowledges financial support from The Swedish Research Council (Grants 621-2009-4736 and 622-2009-371) and computer time from the PDC Center for High Performance Computing. H.A. acknowledges financial support from The Swedish Research Council and from the Carl Trygger Foundation.

Keywords: asymmetric catalysis · density functional calculations · rhodium · hydrogenation · transition states

[1] *Modern Reduction Methods* (Eds.: P. G. Andersson, I. Munslow), Wiley-VCH, Weinheim, **2008**.

[2] a) C. Wang, X. Wu, J. Xiao, *Chem. Asian J.* **2008**, *3*, 1750; b) T. Ikariya, A. J. Blacker, *Acc. Chem. Res.* **2007**, *40*, 1300; c) S. Gladiali, E. Alberico, *Chem. Soc. Rev.* **2006**, *35*, 226; d) J. S. M. Samec, J.-E. Bäckvall, P. G. Andersson, P. Brandt, *Chem. Soc. Rev.* **2006**, *35*, 237; e) T. Ikariya, K. Murata, R. Noyori, *Org. Biomol. Chem.* **2006**, *4*, 393; f) K. Everaere, A. Mortreux, J.-F Carpentier, *Adv. Synth. Catal.* **2003**, *345*, 67; g) T. Ohkuma, R. Noyori in *Comprehensive Asymmetric Catalysis I–III, Vol. 1* (Eds.: E. N. Jacobsen, A. Pfaltz, H. Yamamoto), Springer, Berlin, **1999**, pp. 199; h) M. J. Palmer, M. Wills, *Tetrahedron: Asymmetry* **1999**, *10*, 2045; i) R. Noyori, S. Hashiguchi, *Acc. Chem. Res.* **1997**, *30*, 97; j) G. Zassinovich, G. Mestroni, S. Gladiali, *Chem. Rev.* **1992**, *92*, 1051.

[3] a) S. J. Nordin, P. Roth, T. Tarnai, D. A. Alonso, P. Brandt, P. G. Andersson, *Chem. Eur. J.* **2001**, *7*, 1431; b) D. A. Alonso, S. J. Nordin, P. Roth, T. Tarnai, P. G. Andersson, M. Thommen, U. Pittelkow, *J. Org. Chem.* **2000**, *65*, 3116; c) D. A. Alonso, D. Guijarro, P. Pinho, O. Temme, P. G. Andersson, *J. Org. Chem.* **1998**, *63*, 2749; d) A. Schlatter, W.-D. Woggon, *Adv. Synth. Catal.* **2008**, *350*, 995; e) A. Schlatter, M. K. Kundu, W.-D. Woggon, *Angew. Chem.* **2004**, *116*, 6899; *Angew. Chem. Int. Ed.* **2004**, *43*, 6731; f) M. T. Reetz, X. Li, *J. Am. Chem. Soc.* **2006**, *128*, 1044; g) Y. Jiang, Q. Jiang, X. Zhang, *J. Am. Chem. Soc.* **1998**, *120*, 3817; h) D. S. Matharu, D. J. Morris, A. M. Kawamoto, G. J. Clarkson, M. Wills, *Org. Lett.* **2005**, *7*, 5489; i) T. Jerphagnon, R. Haak, F. Berthiol, A. J. A. Gayet, V. Ritleng, A. Holuigue, N. Pannetier, M. Pfeffer, A. Voelkin, L. Lefort, G. Verzijl, C. Tarabiono, D. B. Janssen, A. J. Minnaard, B. L. Feringa, J. G. de Vries, *Top. Catal.* **2010**, *53*, 1002; j) W. Baratta, F. Benedetti, A. Del Zotto, L. Fanfoni, F. Felluga, S. Magnolia, E. Putignano, P. Rigo, *Organometallics* **2010**, *29*, 3563.

[4] a) M. Yamakawa, I. Yamada, R. Noyori, *Angew. Chem.* **2001**, *113*, 2900; *Angew. Chem. Int. Ed.* **2001**, *40*, 2818; b) R. Noyori, M. Yamakawa, S. Hashiguchi, *J. Org. Chem.* **2001**, *66*, 7931; c) M. Yamakawa, H. Ito, R. Noyori, *J. Am. Chem. Soc.* **2000**, *122*, 1466; d) D. A. Alonso, P. Brandt, S. J. M. Nordin, P. G. Andersson, *J. Am. Chem. Soc.* **1999**, *121*, 9580; e) P. Brandt, P. Roth, P. G. Andersson, *J. Org. Chem.* **2004**, *69*, 4885; f) C. P. Casey, J. B. Johnson, *J. Org. Chem.* **2003**, *68*, 1998.

[5] a) I. M. Pastor, P. Västilä, H. Adolfsson, *Chem. Commun.* **2002**, 2046; b) I. M. Pastor, P. Västilä, H. Adolfsson, *Chem. Eur. J.* **2003**, *9*, 4031; c) A. Bøgevig, I. M. Pastor, H. Adolfsson, *Chem. Eur. J.* **2004**, *10*, 294; d) J. Wet-

tergren, A. B. Zaitsev, H. Adolfsson, *Adv. Synth. Catal.* **2007**, *349*, 2556; e) L. Zani, L. Eriksson, H. Adolfsson, *Eur. J. Org. Chem.* **2008**, 4655.
[6] a) K. Ahlford, A. B. Zaitsev, J. Ekström, H. Adolfsson, *Synlett* **2007**, 2541; b) K. Ahlford, J. Ekström, A. B. Zaitsev, P. Ryberg, L. Eriksson, H. Adolfsson, *Chem. Eur. J.* **2009**, *15*, 11197.
[7] A. B. Zaitsev, H. Adolfsson, *Org. Lett.* **2006**, *8*, 5129.
[8] a) Y. Minenkov, G. Occhipinti, V. R. Jensen, *J. Phys. Chem. A* **2009**, *113*, 11833; b) P. E. M. Siegbahn, M. R. A. Blomberg, S.-L Chen, *J. Chem. Theory Comput.* **2010**, *6*, 2040; c) J. N. Harvey, *Faraday Discuss.* **2010**, *145*, 487; d) C. L. McMullin, J. Jover, J. N. Harvey, N. Fey, *Dalton Trans.* **2010**, *39*, 10833; e) R. Lonsdale, J. N. Harvey, A. J. Mulholland, *J. Phys. Chem. Lett.* **2010**, *1*, 3232; f) S. Osuna, M. Swart, M. Solà, *J. Phys. Chem. A* **2011**, *115*, 3491; g) S. Santoro, R.-Z. Liao, F. Himo, *J. Org. Chem.* **2011**, *76*, 9246.
[9] S. Grimme, *J. Comput. Chem.* **2006**, *27*, 1787.
[10] A. D. Becke, *J. Chem. Phys.* **1993**, *98*, 5648.
[11] Y. Zhao, D. G. Truhlar, *Theor. Chem. Acc.* **2008**, *120*, 215.
[12] Gaussian 03, Revision D.01, M. J. Frisch, G. W. Trucks, H. B. Schlegel, G. E. Scuseria, M. A. Robb, J. R. Cheeseman, J. A. Montgomery, Jr., T. Vreven, K. N. Kudin, J. C. Burant, J. M. Millam, S. S. Iyengar, J. Tomasi, V. Barone, B. Mennucci, M. Cossi, G. Scalmani, N. Rega, G. A. Petersson, H. Nakatsuji, M. Hada, M. Ehara, K. Toyota, R. Fukuda, J. Hasegawa, M. Ishida, T. Nakajima, Y. Honda, O. Kitao, H. Nakai, M. Klene, X. Li, J. E. Knox, H. P. Hratchian, J. B. Cross, V. Bakken, C. Adamo, J. Jaramillo, R. Gomperts, R. E. Stratmann, O. Yazyev, A. J. Austin, R. Cammi, C. Pomelli, J. W. Ochterski, P. Y. Ayala, K. Morokuma, G. A. Voth, P. Salvador, J. J. Dannenberg, V. G. Zakrzewski, S. Dapprich, A. D. Daniels, M. C. Strain, O. Farkas, D. K. Malick, A. D. Rabuck, K. Raghavachari, J. B. Foresman, J. V. Ortiz, Q. Cui, A. G. Baboul, S. Clifford, J. Cioslowski, B. B. Stefanov, G. Liu, A. Liashenko, P. Piskorz, I. Komaromi, R. L. Martin, D. J. Fox, T. Keith, M. A. Al-Laham, C. Y. Peng, A. Nanayakkara, M. Challacombe, P. M. W. Gill, B. Johnson, W. Chen, M. W. Wong, C. Gonzalez, J. A. Pople, Gaussian, Inc., Wallingford CT, **2004**.
[13] D. Andrae, U. Hauessermann, M. Dolg, H. Stoll, H. Preuss, *Theor. Chim. Acta* **1990**, *77*, 123 – 141.
[14] V. Barone, M. Cossi, *J. Phys. Chem. A* **1998**, *102*, 1995.
[15] Gaussian 09, Revision A.02, M. J. Frisch, G. W. Trucks, H. B. Schlegel, G. E. Scuseria, M. A. Robb, J. R. Cheeseman, G. Scalmani, V. Barone, B. Mennucci, G. A. Petersson, H. Nakatsuji, M. Caricato, X. Li, H. P. Hratchian, A. F. Izmaylov, J. Bloino, G. Zheng, J. L. Sonnenberg, M. Hada, M. Ehara, K. Toyota, R. Fukuda, J. Hasegawa, M. Ishida, T. Nakajima, Y. Honda, O. Kitao, H. Nakai, T. Vreven, J. A. Montgomery, Jr., J. E. Peralta, F. Ogliaro, M. Bearpark, J. J. Heyd, E. Brothers, K. N. Kudin, V. N. Staroverov, R. Kobayashi, J. Normand, K. Raghavachari, A. Rendell, J. C. Burant, S. S. Iyengar, J. Tomasi, M. Cossi, N. Rega, J. M. Millam, M. Klene, J. E. Knox, J. B. Cross, V. Bakken, C. Adamo, J. Jaramillo, R. Gomperts, R. E. Stratmann, O. Yazyev, A. J. Austin, R. Cammi, C. Pomelli, J. W. Ochterski, R. L. Martin, K. Morokuma, V. G. Zakrzewski, G. A. Voth, P. Salvador, J. J. Dannenberg, S. Dapprich, A. D. Daniels, Ö. Farkas, J. B. Foresman, J. V. Ortiz, J. Cioslowski, D. J. Fox, Gaussian, Inc., Wallingford CT, **2009**.

Received: January 27, 2012
Published online on April 24, 2012

